IEEE Access
Multidisciplinary | Rapid Review | Open Access Journal

Received 17 February 2023, accepted 26 March 2023, date of publication 31 March 2023, date of current version 6 April 2023.

Digital Object Identifier 10.1109/ACCESS.2023.3263481

RESEARCH ARTICLE

Anti-Saturation Coordination Control of Permanent Magnet Synchronous Wind Power System

DEHAI YU, WEIWEI SUN, XIANGYU CHEN, AND MINGYUAN DU
Institute of Automation, Qufu Normal University, Qufu 273165, China

Corresponding author: Weiwei Sun (wwsun@hotmail.com)

This work was supported in part by the National Natural Science Foundation of China under Grant 62073189 and Grant 62173207, and in part by the Taishan Scholar Project of Shandong Province under Grant tsqn202211129.

ABSTRACT This paper is concerned with the anti-saturation control problem of a permanent magnet synchronous wind power system. By virtue of adaptive sliding mode control method and port-controlled Hamiltonian (PCH) control method, a new coordination controller is designed, which removes the input saturation effects and compensates the uncertainties of system model parameters. The controller takes the exponential function with parameters as the coordination function. By adjusting the parameters of coordination function, the designed coordination controller can respond to input saturation more quickly and improve the system's dynamic performance. The effectiveness of the proposed strategy is demonstrated through simulations. The comparison results with the traditional control approach are also presented. It is shown that the proposed strategy can realize the speed tracking control of the generator and improve the maximum wind energy capture of wind turbine, so as to further improve the utilization efficiency of wind energy.

INDEX TERMS Permanent magnet synchronous wind power generation system, saturation compensation, adaptive sliding mode control, port-controlled Hamiltonian system, coordination control.

I. INTRODUCTION

Wind energy has become an effective resource to solve the energy crisis because of its wide distribution, green, clean and huge accumulation, etc. The most important utilization form of wind energy is wind power, which is the renewable energy with the most mature technology and the most large-scale development prospect at present, and has great value for the sustainable development of society in the context of global environment changes [1]. At present, doubly-fed induction generator (DFIG) and permanent magnet synchronous generator (PMSG) are keys to the wind power generation system at home and abroad. In engineering applications, PMSG is directly connected with the wind turbine shaft, which saves the gearbox compared with DFIG, and reduces the maintenance difficulty of the unit. In addition, PMSG does not need excitation, so it has higher efficiency and operational reliability than the electric excitation generator with the same capacity [2].

Wind power system is a complex energy conversion system with strong nonlinearity. As the wind speed changes rapidly, the optimal speed of the wind turbine also changes rapidly. Due to the inertia of the system, the actual speed of the PMSG will not change instantaneously. In order to achieve fast tracking, the system will generate a large control input, which will lead to input saturation. If we ignore the effect of saturation, the saturation constraint will degrade system performance to some extent or even damage the generator in the PMSG system. In fact, the saturation phenomenon is widespread in practical system, and there are many research results about dealing with actuator saturation recently [3], [4], [5], [6]. In [3], considering the problem of voltage saturation in the control process of a robotic manipulator, the influence of saturation on the control system was eliminated

The associate editor coordinating the review of this manuscript and approving it for publication was Qi Zhou.

by introducing a hyperbolic tangent function to approximate the saturation constraint. In [4], in order to reduce the influence of input saturation constraint on the unmanned surface vessels, an auxiliary dynamic system was constructed, and were estimated external disturbances through a reduced-order extended state observer to improve tracking accuracy and robustness. In [6], a wide area robust damping controller was designed for thyristor controlled series capacitors (TCSC), and the nonlinear effects induced by actuator saturation in closed-loop systems were expressed by a generalized sector condition to enhance the damping of inter-region oscillations in the saturated state of actuators.

In addition to saturation constraint, there are also many unfavorable factors in the operation of PMSG, such as current coupling, model parameter uncertainty and external interference, which seriously restrict the control performance. In view of the uncertain problems that exist in the motor system, the conventional control method is difficult to realize the optimal control for the PMSG system. Some scholars have used the adaptive control method to estimate uncertain parameter disturbances [7], [8], [9], [10] in the application system online, so as to improve the stability and convergence speed of the system. In [8], aiming at the uncertainty of permanent magnet synchronous motor servo system, a new adaptive control method for permanent magnet synchronous motor servo system was proposed. By designing an adaptive law, the uncertainty of parameters was compensated and the convergence speed was improved. In the problem of control for robotic systems with model uncertainty and input time-varying delay, an adaptive controller was designed using the Lyapunov-Krasovskii (L-K) functional method to ensure that the robotic systems could be asymptotically stabilized depending on the input delay in [10].

In recent years, sliding mode control (SMC) [11], [12] and port-controlled Hamiltonian (PCH) control [13], [14] have been applied to the control of power systems and have achieved remarkable results. The PCH control design is relatively simple and has good control effect in terms of control accuracy and system stability, but there exists slow dynamic response speed and poor real-time performance [15]. SMC has good real-time performance, fast response speed, strong robustness, etc, but there is a large output chattering phenomenon in the control process [16], which will reduce the stability of the controlled system. It can be seen that a single control method is difficult to control the system well. By adjusting the control strength of the two control methods, the coordination control strategy not only improves the dynamic response performance and reaches the steady state more quickly, but also improves the control accuracy and steady-state performance of the robotic system in [17]. The coordination control strategy was adopted to solve the control problem of fast and efficiency with the difficult realisation of the motor under a single control method in [18].

To the best of the authors' knowledge, anti-saturation coordination control of wind power generation system has not yet been reported in the literature. Taking full advantage of adaptive sliding mode method and dissipative PCH method, a new coordination control strategy is proposed in this paper for direct-drive PMSG. Compared with the related existing research results, the main contributions and innovations considered in this paper are as follows:

1) A new coordination control strategy is proposed for the PMSG system with input saturation to simultaneously achieve the goal of anti-saturation and compensate for undesirable effects of system model parameters uncertainty.

2) The proposed coordination control strategy is new and the control structure is simple. Under the control strategy, not only the output chattering phenomenon of the sliding mode control is weakened, but also the dynamic performance of the system is improved.

3) A coordination function is chosen in the controller which has two adjustable parameters. This kind of design can coordinate the two control methods (SMC and PCH control) more conveniently and more quickly compared with other design strategies.

The structure of this paper is organized as follows. Section II presents the problem formulation and preliminaries for PMSG systems (modeling of the PMSG and description of the research objective). In Section III, the anti-saturation coordination control scheme of the PMSG system is proposed, and the stability of the system is analyzed. Simulation results are given to verify the validity and feasibility of the designed controller in Section IV. In Section V, the conclusions of this paper and future research directions are given.

II. PROBLEM FORMULATION AND PRELIMINARIES

The direct-drive permanent magnet synchronous wind power system is shown in Fig. 1.

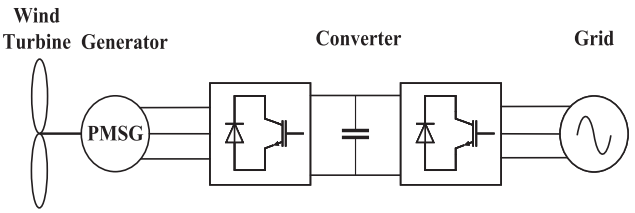

FIGURE 1. Configuration of the PMSG wind turbine.

The mechanical power P_m and aerodynamic torque T_m extracted by a wind turbine from the wind are expressed by the equation [19]

$$\begin{cases} T_m = 0.5\rho\pi R^3 v^2 C_p(\lambda, \beta)/\lambda, \\ P_m = T_m\omega, \\ \lambda = \dfrac{\omega R}{v}, \end{cases} \tag{1}$$

where ρ is the air density, v is the wind speed, R is blade length, C_p is the power coefficient, and ω is the rotor speed. The power coefficient C_p is a function of the tip speed ratio λ and the blade pitch angle β.

The motion equation of the PMSG is

$$J\frac{\mathrm{d}\omega}{\mathrm{d}t} = T_e - T_L - B\omega, \tag{2}$$

where $\omega = \omega_e/p_n$, ω_e is the generator speed, p_n is the number of pole pairs, $T_L = T_m + \Delta_T$ is the mechanical torque of the PMSG, where Δ_T is the uncertain load torque, J is rotational inertia of generator, B is the friction coefficient. The electromagnetic torque of the PMSG is

$$T_e = p_n(\psi_d i_q - \psi_q i_d) = p_n[\psi_f i_q + (L_d - L_q) i_d i_q], \tag{3}$$

where i_d, i_q, L_d, L_q, ψ_d and ψ_q are d-axis and q-axis components of stator current, stator inductance and equivalent flux linkage of generator, respectively. ψ_f is the flux linkage of the permanent magnets, L_s is the stator inductance. In the non-salient pole PMSG case ($L_d = L_q = L$), the electromagnetic torque is written as

$$T_e = p_n \psi_f i_q. \tag{4}$$

For direct-drive permanent magnet synchronous wind power systems, the model of the PMSG can be described in the d-q synchronously rotating reference frame as

$$\begin{cases} L_d \dfrac{\mathrm{d}i_d}{\mathrm{d}t} = -R_s i_d + p_n \omega L_q i_q + u_d, \\ L_q \dfrac{\mathrm{d}i_q}{\mathrm{d}t} = -R_s i_q - p_n \omega L_d i_d - p_n \omega \psi_f + u_q, \\ J\dfrac{\mathrm{d}\omega}{\mathrm{d}t} = T_e - T_L - B\omega, \\ \dfrac{\mathrm{d}\theta}{\mathrm{d}t} = \omega, \end{cases} \tag{5}$$

where u_d and u_q are d-axis and q-axis components of stator voltages, respectively, R_s is stator resistance, θ is position of rotor, $(\bar{i}_d, \bar{i}_q, \omega_r)$ is the desired equilibrium point of the PMSG system, and $\bar{i}_d$, $\bar{i}_q$ and ω_r are d-axis and q-axis components of currents and gener speed at the desired equilibrium point, respectively.

The motivation of this paper is to design a coordination controller for the system (5) considering saturation and model parameter uncertainty. The proposed controller can eliminate the influence of input saturation quickly, track the input speed and improve the stability of the system. In detail, the design process will be divided into three steps: Firstly, design an adaptive sliding mode controller to solve the problem of current saturation and parameter uncertainty in the system, so that the system can reach the steady-state quickly. Secondly, the controller based on the PCH model is designed to improve the steady-state performance of the PMSG system. Thirdly, through coordination function c_s and c_e, the final coordination controller u_d and u_q are obtained to achieve the maximum wind energy capture of the wind turbine and improve the efficiency of wind energy utilization.

III. CONTROLLERS DESIGN

A. ADAPTIVE SLIDING MODE CONTROLLER DESIGN

Based on the backstepping method, an adaptive sliding controller is designed in this part. The controller is insensitive to external parameters and has strong robustness, which is used to enhance the steady-state performance of the system. In addition, since the friction coefficient has little influence on the system, in order to simplify the design of the controller, we take the coefficient of friction $B = 0$.

Step 1: Given desired value of speed be ω_r, the speed tracking error of the PMSG system is $e_\omega = \omega_r - \omega$. Its derivative along the trajectories of (5) is as follows:

$$\dot{e}_\omega = \dot{\omega}_r - \dot{\omega} = \dot{\omega}_r - \frac{1}{J}(p_n \psi_f i_q - T_L). \tag{6}$$

Defining the state variable

$$\begin{cases} x_{s1} = e_\omega = \omega_r - \omega, \\ x_{s2} = \int_0^t x_{s1}\mathrm{d}t = \int_0^t (\omega_r - \omega)\mathrm{d}t, \end{cases} \tag{7}$$

we introduce the following sliding surface:

$$s = x_{s1} + c x_{s2}, \tag{8}$$

where c is the integral constant and $c > 0$. By computing the differential of s along the trajectories of (5), we obtain the following equality:

$$\dot{s} = \dot{x}_{s1} + c\dot{x}_{s2} = \dot{\omega}_r + \frac{T_L}{J} - \frac{p_n \psi_f i_q}{J} + c e_\omega = \nu - M\vartheta, \tag{9}$$

where $\nu = -\frac{1}{J} p_n \psi_f i_q$ is the intermediate control variate, $M = [-(\dot{\omega}_r + c e_\omega) \ -1]$, $\vartheta = \frac{1}{J}[J \ T_L]^{\mathrm{T}}$ is the parameter matrix to be estimated, which contains uncertain parameter T_L.

Putting the system input saturation aside and only considering the model parameter uncertainty, we can obtain the virtual control law

$$\nu = M\hat{\vartheta} - \varepsilon f(s)\mathrm{sgn}(s) - k_1 s, \tag{10}$$

where $\hat{\vartheta} \in \mathbb{R}^2$ is the estimated value of the uncertainty parameter matrix ϑ, $\varepsilon > 0$, $k_1 > 0$, $f(s) = \frac{1}{1+\frac{1}{|s+1|}}$ and the function $f(s)$ is strictly positive definite.

From (9) and (10), the control current can be obtained

$$i_{qr} = -\frac{J}{p_n \psi_f}(M\hat{\vartheta} - \varepsilon f(s)\mathrm{sgn}(s) - k_1 s). \tag{11}$$

Adaptation law is designed as follows:

$$\dot{\hat{\vartheta}} = -\Gamma M^{\mathrm{T}} s, \tag{12}$$

where $\Gamma = \mathrm{diag}\{\gamma_{11}, \gamma_{22}\}$, $\gamma_{11}, \gamma_{22} > 0$.

Select the Lyapunov function as follows:

$$V_0 = \frac{1}{2}s^2 + \frac{1}{2}\tilde{\vartheta}^{\mathrm{T}}\Gamma^{-1}\tilde{\vartheta}, \tag{13}$$

where $\tilde{\vartheta} = \vartheta - \hat{\vartheta}$ is the estimation error.

Combining (9), (10), and (12), the derivative of V_0 can be derived as follows:

$$\begin{aligned} \dot{V}_0 &= s\dot{s} + \tilde{\vartheta}^{\mathrm{T}}\Gamma^{-1}\dot{\tilde{\vartheta}} \\ &= s(\nu - M\hat{\vartheta}) - \tilde{\vartheta}^{\mathrm{T}}\Gamma^{-1}(\dot{\hat{\vartheta}} + \Gamma M^{\mathrm{T}} s) \\ &= -k_1 s^2 - \varepsilon f(s)|s|. \end{aligned} \tag{14}$$

From (13), (14), and $s = x_{s1} + cx_{s2}$, it can be known that the tracking error x_{s1}, the velocity error x_{s2}, and the parameter estimation error $\tilde{\vartheta}$ are globally uniformly bounded. Because $\tilde{\vartheta} = \vartheta - \hat{\vartheta}$, the estimated parameter $\hat{\vartheta}$ is also globally uniformly bounded. Taking the derivative of equation (14) yields $\ddot{V}_0 = -2k_1 s\dot{s}$, so $\dot{V}_0$ is bounded, and it is concluded that V_0 is uniformly continuous. According to Barbalat Lemma: If function $\phi : \mathbb{R}_+ \to \mathbb{R}$ is uniformly continuous, and the $\lim_{t\to\infty} \int_0^t \phi(s)\mathrm{d}s$ exists and is finite, then $\lim_{t\to\infty} \phi(t) = 0$, it can be known that the tracking error e_ω will tend to zero with time t, which means that the system output ω will converge to the reference track ω_r with time t.

When the wind speed changes rapidly, the reference speed of the system's input changes rapidly, so the speed error e_ω also increases. In order to achieve the effect of fast tracking, the system may have a large control input, resulting in input saturation of the control current, which may affect the stability of the control system if not controlled. So we need to design an anti-saturation control law to make the system stable. q-axis input current saturation constraint is as follows:

$$i_{qr} = \mathrm{sat}(i_{qr}^*) = \begin{cases} i_{qrM}^*, & i_{qr}^* \geq i_{qrM}^*, \\ i_{qr}^*, & i_{qrm}^* \leq i_{qr}^* \leq i_{qrM}^*, \\ i_{qrm}^*, & i_{qr}^* \leq i_{qrm}^*, \end{cases} \tag{15}$$

where i_{qrm}^*, i_{qrM}^* are positive constants, and i_{qr}^* is the control input to be designed, in order to design the control law of i_{qr}^*, the following auxiliary design system is introduced [20]:

$$\dot{\chi} = \begin{cases} -\zeta\chi - \dfrac{|sK\Delta i_{qr}| + \frac{1}{2}\Delta i_{qr}^2}{\chi} + \Delta i_{qr}, & |\chi| \geq \delta, \\ 0, & |\chi| < \delta, \end{cases} \tag{16}$$

where $\chi \in \mathbb{R}$ is the state of the auxiliary design system, $\zeta > 0, K = \frac{1}{J} p_n \psi_f$, $\Delta i_{qr} = i_{qr} - i_{qr}^*$, δ is a positive constant.

When the input saturation characteristic of the system is considered, according to (15) and (16), the control current can be obtained as

$$i_{qr}^* = -\frac{J}{p_n\psi_f}(M\hat{\vartheta} - \varepsilon f(s)\mathrm{sgn}(s) - k_1 s - \eta\chi), \tag{17}$$

where η is a positive constant. As can be seen from (17), when input saturation occurs in the system, i_{qr}^* will be updated continuously through the compensation term χ to limit the value of i_{qr}^* within the saturation constraint and level off to i_{qr}, i.e., the excess part of the system control input current is compensated.

When $|\chi| \geq \delta$, we select the Lyapunov function

$$V_1 = V_0 + \frac{1}{2}\chi^2. \tag{18}$$

Combining (13) and (16), the derivative of V_1 can be derived as follows:

$$\begin{aligned} \dot{V}_1 &= V_0 + \chi\dot{\chi} \\ &= V_0 + \chi\left(-\frac{|sK\Delta i_{qr}| + \frac{1}{2}\Delta i_{qr}^2}{\chi} - \zeta\chi + \Delta i_{qr}\right) \\ &= V_0 - \zeta\chi^2 - |sK\Delta i_{qr}| - \frac{1}{2}\Delta i_{qr}^2 + \Delta i_{qr}\chi. \end{aligned} \tag{19}$$

According to average value inequality, we have

$$\Delta i_{qr}\chi \leq \frac{1}{2}\Delta i_{qr}^2 + \frac{1}{2}\chi^2. \tag{20}$$

Then substituting (14) and (20) into (19), the following inequality can be obtained

$$\begin{aligned} \dot{V}_1 &\leq -k_1 s^2 - \varepsilon f(s)|s| - (\zeta - \frac{1}{2})\chi^2 - |s \cdot K \cdot \Delta i_{qr}| \\ &\leq -k_1 s^2 - \varepsilon f(s)|s| - (\zeta - \frac{1}{2})\chi^2. \end{aligned} \tag{21}$$

Take $\zeta > \frac{1}{2}$, then $\dot{V}_1 < 0$. From (21), we can conclude that the system (5) is asymptotically stable under the control law (17). As $s = x_{s1} + cx_{s2}$ and $c > 0$, it can be seen from (18) and (21) that e_ω and $\dot{e}_\omega$ are globally uniformly bounded. According to Barbalat Lemma, it can be known that the tracking error e_ω will tend to zero with time t, which means that the system output ω will converge to the reference track ω_r with time t.

It is worth pointing out that the above analysis only contains the result when the states of the auxiliary design system (16) satisfy the condition $|\chi| > \delta$, i.e., there exists input saturation. If $|\chi| < \delta$, it means that there does not exist input saturation, we have $\Delta i_{qr} = 0$, i.e., $i_{qr} = i_{qr}^*$ and the control input i_{qr} is bounded. Thus, i_{qr}^* is bounded. The stability analysis can be easily proved by considering equations (18)-(21) when $|\chi| < \delta$.

Step 2: Defining q-axis current tracking error $e_q = i_{qr}^* - i_q$, taking the derivative of it and combining (5), we have

$$\begin{aligned} \dot{e}_q &= \dot{i}_{qr}^* - \dot{i}_q \\ &= \dot{i}_{qr}^* - \frac{1}{L_s}(u_q - R_s i_q - p_n\omega L_s i_d - p_n\omega\psi_f). \end{aligned} \tag{22}$$

Let $\dot{e}_q = -k_{sq}e_q$, where $k_{sq} > 0$. Combined with the above equation, the actual control item u_{sq} of q-axis voltage u_q can be obtained as

$$\begin{aligned} u_{sq} = (R_s - L_s k_{sq})i_q + p_n\omega L_s i_d + p_n\omega\psi_f \\ + L_s\dot{i}_{qr}^* + L_s k_{sq} i_{qr}^*. \end{aligned} \tag{23}$$

Selecting the Lyapunov function $V_2 = V_1 + \frac{1}{2}{e_q}^2$, and combining (21), we get

$$\begin{aligned} \dot{V}_2 &= \dot{V}_1 + e_q\dot{e}_q \\ &\leq -\varepsilon f(s)|s| - k_1 s^2 - (\zeta - \frac{1}{2})\chi^2 - k_{sd}{e_q}^2 < 0. \end{aligned} \tag{24}$$

Step 3: Define d-axis current tracking error $e_d = i_{dr}^* - i_d$. Taking the derivative of it and combining (5), it yields

$$\dot{e}_d = \dot{i}_{dr}^* - \dot{i}_d = \dot{i}_{dr}^* - \frac{1}{L_s}(u_d - R_s i_d + p_n\omega L_s i_q). \tag{25}$$

Let $\dot{e}_d = -k_{sd}e_d$, where $k_{sd} > 0$. Combined with the above equation, the actual control item u_{sd} of u_d can be obtained as

$$u_{sd} = (R_s - L_s k_{sd})i_d - p_n\omega L_s i_q + L_s\dot{i}_{dr}^* + L_s k_{sd} i_{dr}^*. \tag{26}$$

Selecting the Lyapunov function $V_3 = V_2 + \frac{1}{2}e_d{}^2$, and combining (24), we get

$$\begin{aligned}\dot{V}_3 &= \dot{V}_2 + e_d\dot{e}_d \\ &\le -\varepsilon f(s)|s| - k_1 s^2 - (\zeta - \frac{1}{2})\chi^2 - k_{sq}e_q{}^2 - k_{sd}e_d{}^2 \\ &< 0.\end{aligned} \tag{27}$$

In conclusion, the adaptive sliding mode controller of the system is designed as

$$\begin{cases} u_{sd} = (R_s - L_s k_{sd})i_d - p_n\omega L_s i_q + L_s\dot{i}_{dr}^* \\ \qquad + L_s k_{sd} i_{dr}^*, \\ u_{sq} = (R_s - L_s k_{sq})i_q + p_n\omega L_s i_d + p_n\omega\psi_f \\ \qquad + L_s\dot{i}_{qr}^* + L_s k_{sq} i_{qr}^*, \end{cases} \tag{28}$$

where $\dot{i}_{dr}^* = 0$, $\dot{i}_{qr}^* = -\frac{J}{p_n\psi_f}(M\dot{\hat{\vartheta}} - k_1\dot{s} - \eta\dot{\chi} - \varepsilon f(s)\mathrm{sgn}(s))$, where the analytic expressions of $\dot{s}$, $\dot{\hat{\vartheta}}$ and $\dot{\chi}$ are given by (9), (12) and (16) respectively.

B. CONTROLLER DESIGN BASED ON PCH MODEL

In this subsection, we propose a PCH model-based controller for system (5).

Take $D = \mathrm{diag}\{L_d, L_q, J\}$ and let the system state vector x, the input vector u and the output vector y be as follows:

$$\begin{aligned} x &= \begin{bmatrix} x_1 \\ x_2 \\ x_3 \end{bmatrix} = \begin{bmatrix} L_d i_d \\ L_q i_q \\ J\omega \end{bmatrix} = D\begin{bmatrix} i_d \\ i_q \\ \omega \end{bmatrix}, \\ u &= \begin{bmatrix} u_{ed} \\ u_{eq} \\ -T_L \end{bmatrix}, \\ y &= \begin{bmatrix} i_d \\ i_q \\ \omega \end{bmatrix} \end{aligned} \tag{29}$$

Select the Hamiltonian function as

$$H(x) = \frac{1}{2}x^{\mathrm{T}}D^{-1}x = \frac{1}{2}(\frac{1}{L_s}x_1{}^2 + \frac{1}{L_s}x_2{}^2 + \frac{1}{J}x_3{}^2), \tag{30}$$

then the system (5) can be modeled as the following PCH model:

$$\begin{cases} \dot{x} = [J(x) - R(x)]\dfrac{\partial H(x)}{\partial x} + g(x)u, \\ y = g^{\mathrm{T}}(x)\dfrac{\partial H(x)}{\partial x}, \end{cases} \tag{31}$$

where

$$J(x) = \begin{bmatrix} 0 & 0 & p_n x_2 \\ 0 & 0 & -p_n(x_1 + \psi_f) \\ -p_n x_2 & p_n(x_1 + \psi_f) & 0 \end{bmatrix},$$

$$R(x) = \mathrm{diag}\{R_s, R_s, 0\}, \quad g(x) = \mathrm{diag}\{1, 1, 1\}. \tag{32}$$

Obviously, $J(x) \in \mathbb{R}^{3\times3}$ is an antisymmetric matrix, which reflects the internally interconnected structure of the system, $R(x) \in \mathbb{R}^{3\times3}$ is a positive semi-definite matrix, which reflects the additional resistive structure of port, $g(x)$ reflects the port characteristics of the system, and its matrix form is determined by the mathematical model of the controlled system.

Let $\bar{x} = [L_d\bar{i}_d \;\; L_q\bar{i}_q \;\; J\omega_r]^{\mathrm{T}}$ be the desired equilibrium point of the system (31). Through the energy shaping and controller design for the system (31), the system can operate stably at the desired equilibrium $\bar{x}$. Therefore, the actual speed ω in the system (5) can track the desired speed ω_r, achieving the maximum wind energy capture of the wind turbine and improving the utilization rate of wind energy. For a surface-mounted PMSG, in order to satisfy the control principle of "Maximum torque/current", the control of $\bar{i}_d = 0$ is usually adopted when the system operates at the equilibrium point.

A new Hamiltonian energy function $H_d(x)$ is constructed to achieve the minimum value at $\bar{x}$, and a feedback control law $u = \alpha(x)$ is introduced, so the closed-loop system (31) can be rewritten as

$$\dot{x} = [J_d(x) - R_d(x)]\frac{\partial H_d(x)}{\partial x} \tag{33}$$

which satisfies the partial differential equation

$$\begin{aligned}[J_d(x) - R_d(x)]\frac{\partial H_a(x)}{\partial x} = -[J_a(x) - R_a(x)]\frac{\partial H(x)}{\partial x} \\ + g(x)\alpha(x),\end{aligned} \tag{34}$$

where $H_a(x) = H_d(x) - H(x)$ is the external energy injected into the system, $J_d(x) = J_a(x) + J(x) = -J_d^{\mathrm{T}}(x)$ and $R_d(x) = R_a(x) + R(x) = R_d^{\mathrm{T}}(x) \ge 0$ are the desired interconnection and damping matrices, respectively, and

$$\begin{cases} \dfrac{\partial H(x)}{\partial x} = D^{-1}x, \\ \dfrac{\partial H_a(x)}{\partial x} = \dfrac{\partial H_d(x)}{\partial x} - \dfrac{\partial H(x)}{\partial x} = -D^{-1}\bar{x}. \end{cases} \tag{35}$$

For the system (33), the desired Hamiltonian energy function is defined as

$$\begin{aligned}H_d(x) = \frac{1}{2}(x - \bar{x})^{\mathrm{T}}D^{-1}(x - \bar{x}) = \frac{1}{2}(\frac{1}{L_s}(x_1 - \bar{x}_1)^2 \\ + \frac{1}{L_s}(x_2 - \bar{x}_2)^2 + \frac{1}{J}(x_3 - \bar{x}_3)^2).\end{aligned} \tag{36}$$

The interconnection matrix and damping matrix in the closed-loop system (33) are chosen as

$$\begin{aligned} J_a(x) &= \begin{bmatrix} 0 & -J_{12} & J_{13} \\ J_{12} & 0 & -J_{23} \\ -J_{13} & J_{23} & 0 \end{bmatrix}, \\ R_a(x) &= \begin{bmatrix} r_1 & 0 & 0 \\ 0 & r_2 & 0 \\ 0 & 0 & 0 \end{bmatrix}. \end{aligned} \tag{37}$$

Substituting (29), (32), (35) and (37) into (34) yields

$$\begin{cases} u_{ed} = -r_1 i_d - J_{12} i_q + J_{13}\omega + (R_s + r_1)\bar{i}_d + J_{12} \\ \qquad \cdot \bar{i}_q - (J_{13} + p_n x_2)\omega_r, \\ u_{eq} = J_{12} i_d - r_2 i_q - J_{23}\omega - J_{12}\bar{i}_d + (R_s + r_2)\bar{i}_q \\ \qquad + (J_{23} + p_n(x_1 + \psi_f))\omega_r, \\ T_L = J_{13} i_d - J_{23} i_q - (J_{13} + p_n x_2)\bar{i}_d + (J_{23} + p_n \\ \qquad \cdot (x_1 \psi_f))\bar{i}_q. \end{cases} \tag{38}$$

Choosing $J_{13} = -\frac{L_d}{L_q} p_n x_2$, $J_{23} = -p_n x_1$, $J_{12} = 0$ and substituting them into (38), we get

$$\begin{cases} u_{ed} = -r_1 i_d - p_n L_s i_q \omega, \\ u_{eq} = -r_2 i_q + p_n L_s i_d \omega + (R_s + r_2)\bar{i}_q + p_n \psi_f \omega_r. \end{cases} \tag{39}$$

When T_L is known, we know from the system (5)

$$\begin{cases} \dot{\theta} = \omega, \\ \dot{\omega} = \dfrac{p_n \psi_f i_q}{J} - \dfrac{T_L}{J}, \\ \dot{T}_L = 0. \end{cases} \tag{40}$$

However, in practice, T_L is usually uncertain and needs to be estimated. Since the speed and current in the system can be measured, the torque observer can be constructed by error feedback

$$\begin{cases} \dot{\hat{\theta}} = \hat{\omega} + a_1(\theta - \hat{\theta}), \\ \dot{\hat{\omega}} = \dfrac{p_n \psi_f i_q}{J} - \dfrac{\hat{T}_L}{J} + a_2(\theta - \hat{\theta}), \\ \dot{\hat{T}}_L = a_3(\theta - \hat{\theta}), \end{cases} \tag{41}$$

where a_1, a_2 and a_3 are design parameters.

Define the estimation error

$$\tilde{\theta} = \theta - \hat{\theta}, \tilde{\omega} = \omega - \hat{\omega}, \tilde{T}_L = T_L - \hat{T}_L.$$

According to (40) and (41), we can obtain the error dynamic equation as follows:

$$\begin{bmatrix} \dot{\tilde{\theta}} \\ \dot{\tilde{\omega}} \\ \dot{\tilde{T}}_L \end{bmatrix} = \begin{bmatrix} -a_1 & 1 & 0 \\ -a_2 & 0 & -\dfrac{1}{J} \\ -a_3 & 0 & 0 \end{bmatrix} \begin{bmatrix} \tilde{\theta} \\ \tilde{\omega} \\ \tilde{T}_L \end{bmatrix}. \tag{42}$$

The characteristic equation of the load observer is

$$s^3 + a_1 s^2 + a_2 s - \frac{a_3}{J} = 0.$$

According to the Routh Criterion, the system (42) is asymptotically stable when $a_1 > 0$, $a_2 > 0$, $-Ja_1 a_2 < a_3 < 0$.

Assuming that all the poles of the observer are set at s_p, where $s_p < 0$, it follows from the above equation:

$$a_1 = -3s_p, \quad a_2 = 3s_p^2, \ a_3 = Js_p^3.$$

Thus, the estimation error of T_L decays exponentially to zero.

By the estimation of T_L, it can be known from (4) that when the system (31) operates at the desired equilibrium point, we have

$$\hat{i}_q = \frac{\hat{T}_L}{p_n \psi_f}.$$

Therefore, the PCH model-based controller is designed as

$$\begin{cases} u_{ed} = -r_1 i_d - p_n L_s i_q \omega, \\ u_{eq} = -r_2 i_q + p_n L_s i_d \omega + (R_s + r_2)\dfrac{\hat{T}_L}{p_n \psi_f} \\ \qquad + p_n \psi_f \omega_r. \end{cases} \tag{43}$$

C. COORDINATION CONTROLLER DESIGN

In this subsection, based on the above two control methods, a new coordination controller is designed, which can reduce the chattering phenomenon caused by sliding mode control to a certain extent. The control strategy improves the response speed and steady-state performance, and thus increases the utilization rate of wind energy. Table 1 briefly describes the characteristics of the three control methods.

TABLE 1. The characteristics of control methods.

Control Methods	Characteristics
Sliding Mode Control	fast dynamic response speed strong robustness output chattering
PCH Control	excellent stability slow dynamic response speed
Coordination Control	fast dynamic response speed excellent stability output chattering is weakened

Define $c_{sd}(t), c_{ed}(t), c_{sq}(t), c_{eq}(t)$ as the coordination functions of the coordination controller. Set $|\omega_r - \omega| > \epsilon$, where ϵ is a positive constant, the start time is t_i. When detect speed error of system (5) has large fluctuation and saturation occurs, the adaptive sliding mode control plays the main role by adjusting the parameters of coordination controller, and the system quickly reaches the steady state through saturation compensation. Therefore, we design the coordination function as follows:

$$\begin{cases} c_{sd}(t) = c_{sq}(t) = e^{-h(t-t_i)^{2k}}, \\ c_{ed}(t) = c_{eq}(t) = 1 - e^{-h(t-t_i)^{2k}}, \end{cases} \tag{44}$$

where h, k are known constants, $h \geq 0$, $k = 2, 3, 4\cdots$, and $c_{sd}(t), c_{ed}(t), c_{sq}(t), c_{eq}(t) \in [0, 1]$.

For the system (5), we design the coordination controller as

$$\begin{cases} u_d = c_{sd}(t) u_{sd} + c_{ed}(t) u_{ed}, \\ u_q = c_{sq}(t) u_{sq} + c_{eq}(t) u_{eq}, \end{cases} \tag{45}$$

where u_{sd}, u_{sq} and u_{ed}, u_{eq} are given by (28) and (39) respectively.

Remark 1: When the parameter h is fixed and $k = 1$, the adaptive sliding mode controller plays the main role in the initial operation of the system. After the system reaches the steady state, the controller based on PCH model only works for a short time and cannot achieve the function of controlling the system with small energy loss at steady state. When $k \to \infty$, the adaptive sliding mode controller plays the main control role for a long time, which can not reflect the fast tracking effect of coordination control, and can not reflect that coordination control that makes the system reach the steady state faster. When the parameter k is fixed, the larger the value of h is, the shorter the time for the adaptive sliding mode controller to act as the main control. On the contrary, the smaller the value of h is, the longer the time for the adaptive sliding mode controller plays the main control role, which can not reflect the fast response performance of the coordination controller.

An example is given to verify the effect of changes the parameters k and h on the coordination function. Given parameters $k = 2$ and $h = 100$, the simulation waveform of the example shows the influence of the changes of h and k on the coordination function consistent with the above analysis. The simulation waveform is shown in Fig. 2.

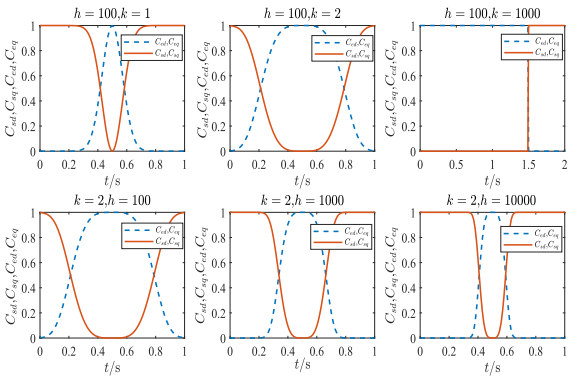

FIGURE 2. Comparison waveforms of coordination function under different parameters.

Therefore, in order to make the two control methods cooperate better and achieve an ideal control effect, the value of h and k should be adjusted in the simulation test of the system according to the actual demand to make the system reach the desired stable operation state.

Based on the above analysis, to maintain the stable operation of the PMSG system with input saturation and parameter uncertainty, a coordination controller is designed. The theorem is follows:

Theorem 1: Considering the PMSG system (5), a coordination controller (45) is designed to make the closed-loop system asymptotically stable under input saturation and parameter uncertainty so as to ensure that the output speed of PMSG can track the expected speed, to achieve the maximum wind energy capture of the wind turbine and improve the utilization efficiency of wind energy.

Proof: For the two cases of input saturation and model parameter uncertainty, the stability analysis of the system (5) is carried out under the coordination controller (45) by selecting an appropriate coordination function (44). Therefore, the Lyapunov function of the system (5) can be selected as

$$V = V_3 + \frac{1}{2}(x - \bar{x})^{\mathrm{T}} D^{-1}(x - \bar{x}). \tag{46}$$

Since $J_d(x)$ is an antisymmetric matrix, we have

$$(\frac{\partial H_d(x)}{\partial x})^{\mathrm{T}} J_d(x) \frac{\partial H_d(x)}{\partial x} = 0.$$

Substitute (27) into (46) and take the derivative of it

$$\begin{aligned}
\dot{V} &= \dot{V}_3 + (\frac{\partial H_d(x)}{\partial x})^{\mathrm{T}} \dot{x} \\
&= \dot{V}_3 + (\frac{\partial H_d(x)}{\partial x})^{\mathrm{T}} [J_d(x) - R_d(x)] \frac{\partial H_d(x)}{\partial x} \\
&\leq -k_1 s^2 - \varepsilon f(s)|s| - (\zeta - \frac{1}{2})\chi^2 - k_{sq} e_q^2 - k_{sd} e_d^2 \\
&\quad - (\frac{\partial H_d(x)}{\partial x})^{\mathrm{T}} R_d(x) \frac{\partial H_d(x)}{\partial x} \\
&\leq -(\frac{\partial H_d(x)}{\partial x})^{\mathrm{T}} R_d(x) \frac{\partial H_d(x)}{\partial x}.
\end{aligned} \tag{47}$$

Since R_d is positive semi-definite, one gets

$$(\frac{\partial H_d(x)}{\partial x})^{\mathrm{T}} R_d(x) \frac{\partial H_d(x)}{\partial x} > 0.$$

It is easy to know that V is positive definite and $\dot{V}$ is negative semi-definite. According to LaSalle's principle, if the maximum invariant set of the system (33) is $\{\bar{x}\}$ and is contained in the set

$$\{x \in \mathbb{R}^n | (\frac{\partial H_d(x)}{\partial x})^{\mathrm{T}} R_d(x) \frac{\partial H_d(x)}{\partial x} = 0\},$$

then it can be proved that the system (31) is asymptotically stable at the equilibrium point $\bar{x}$.

According to Lyapunov stability theorem, we can conclude that the closed-loop system (5) under the coordination controller (45) is asymptotically stable. This completes the proof.

IV. SYSTEM SIMULATION RESULTS AND ANALYSIS

In order to verify the effectiveness of the designed coordination controller, the permanent magnet synchronous wind power system with saturation and uncertain model parameters is simulated in Matlab/Simulink environment. The system control block diagram is shown in Fig. 3.

The parameters of the PMSG are shown in Table 2, and the parameters of the controller are shown in Table 3.

The limit of control input current saturation is ± 4 A. Wind speed is set as

$$v = \begin{cases} 6 \text{ m/s}, & 0s \leq t < 3\ s, \\ 18 \text{ m/s}, & 3s \leq t < 6\ s, \\ 12 \text{ m/s}, & 6s \leq t \leq 10\ s. \end{cases}$$

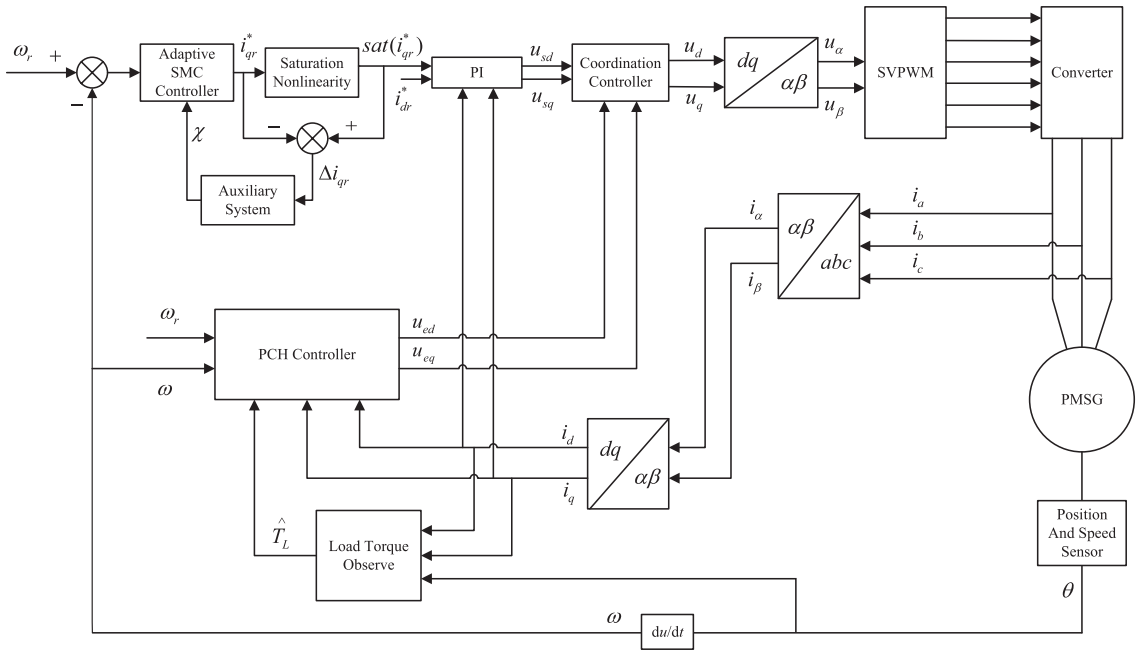

FIGURE 3. System anti-saturation coordination control block diagram.

TABLE 2. Specification of the PMSG.

PMSG parameters			Wind turbine parameters		
Parameters	**Symbol**	**Value**	**Parameters**	**Symbol**	**Value**
Rated power (kW)	P_n	4.5	Air density (kg/m^3)	ρ	1.25
Rated voltage (V)	U_n	380	Optimum tip speed ratio	λ_{opt}	8.1
Rated frequency (Hz)	f	50	Turbine blade radius (m)	R	5
Stator resistance (Ω)	R_s	2.875	Maximum power coefficient	C_p	0.48
Stator inductance (H)	L_d,L_q	8.5×10^{-3}			
Rotational inertia ($kg \cdot m^2$)	J	8×10^{-3}			
Pole pairs number	p_n	5			
Permanent magnetic flux (Wb)	ψ_f	0.175			
Friction coefficient ($N \cdot m \cdot s$)	B	0			

TABLE 3. Controller parameters.

Parameters	k_1	c	a_1	ε	γ_{11}	γ_{22}	γ_{22}	k_{sq}
Value	2	200	0.8	100	0.1	1	1000	1000
Parameters	ζ	η	δ	r_1	r_2	s_p	h	k
Value	10	900	0.1	0.1	0.1	-100	800	2

According to the principle of wind turbine characteristics, in order to track the maximum power point, the desired optimal speed is as follows:

$$\omega_r = \frac{\lambda_{opt} v}{R} = \frac{8.1\ v}{R}. \tag{48}$$

According to (48), the desired speed ω_r under different wind speeds can be calculated as

$$\omega_r = \begin{cases} 9.72\ \text{rad/s}, & 0\text{s} \le t < 3\text{s}, \\ 29.16\ \text{rad/s}, & 3\text{s} \le t < 6\text{s}, \\ 19.44\ \text{rad/s}, & 6\text{s} \le t \le 10\text{s}. \end{cases}$$

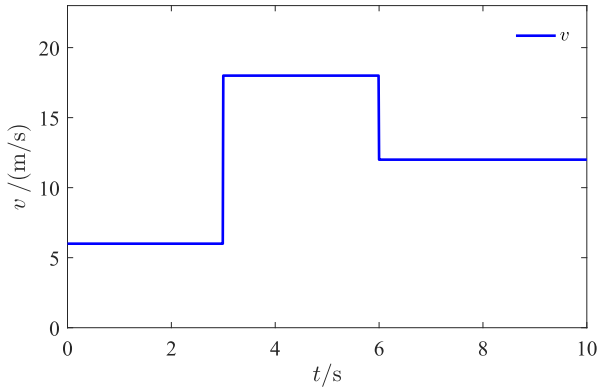

FIGURE 4. Curve of the wind turbine input wind speed.

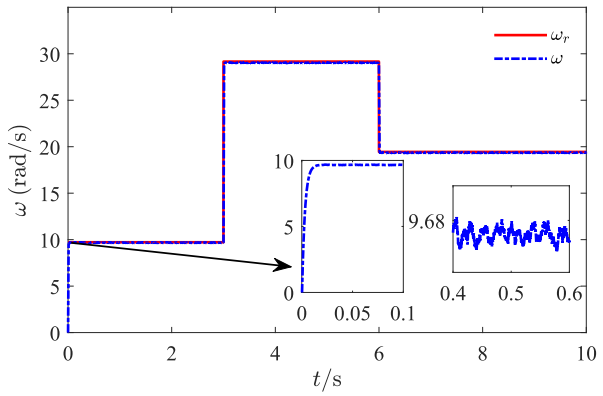

FIGURE 5. Speed curve of adaptive sliding mode anti-saturation control.

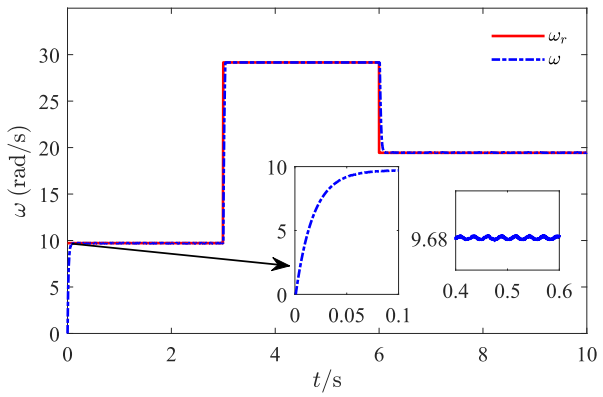

FIGURE 6. Speed curve of PCH model-based control.

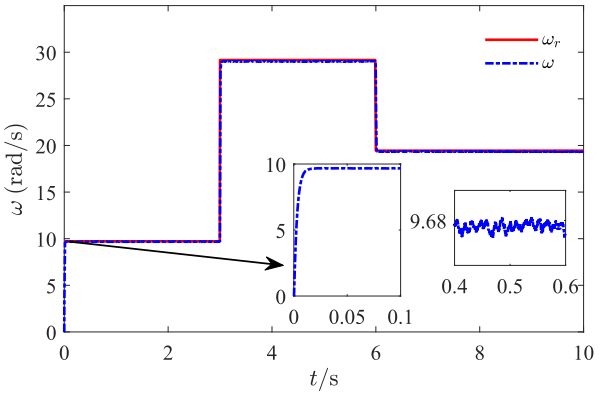

FIGURE 7. Active disturbance rejection and sliding mode coordination control speed curve.

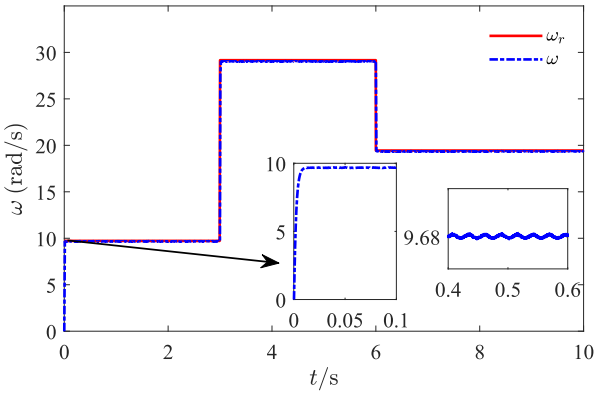

FIGURE 8. Coordination control speed curve.

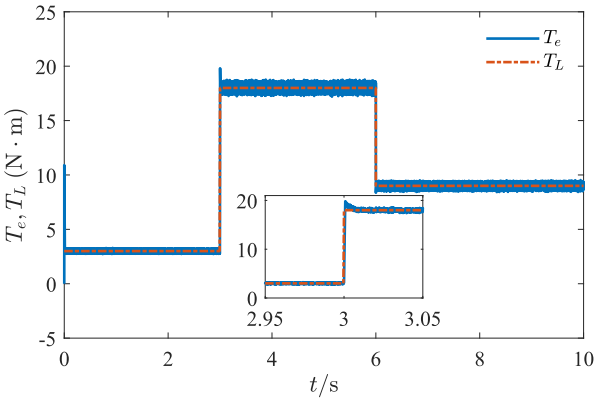

FIGURE 9. Coordination control electromagnetic torque curve.

Assuming that the initial wind speed is 6 m/s, it suddenly changes to 18 m/s at 3 s, and again changes to 12 m/s at 6 s. Then the curve of wind speed change is shown in Fig. 4.

A. SIMULATION OF THE PMSG SYSTEM WITHOUT INPUT SATURATION

First of all, the saturation constraint of the convertor current at the machine side is not considered. At this time, the anti-saturation auxiliary system does not work. Simulation results are shown in Figs. 5-11.

Fig. 5 shows that when the adaptive sliding mode anti-saturation controller acts alone, the PMSG can quickly track the given desired speed, but the output has chattering problem to some extent. It can be seen from Fig. 6 that compared with Fig. 5, when the controller based on PCH model acts alone, the system output is stable, but the response speed is slower. Fig. 7 shows the speed output waveform of the PMSG system under the coordinated controller composed of active disturbance rejection and sliding

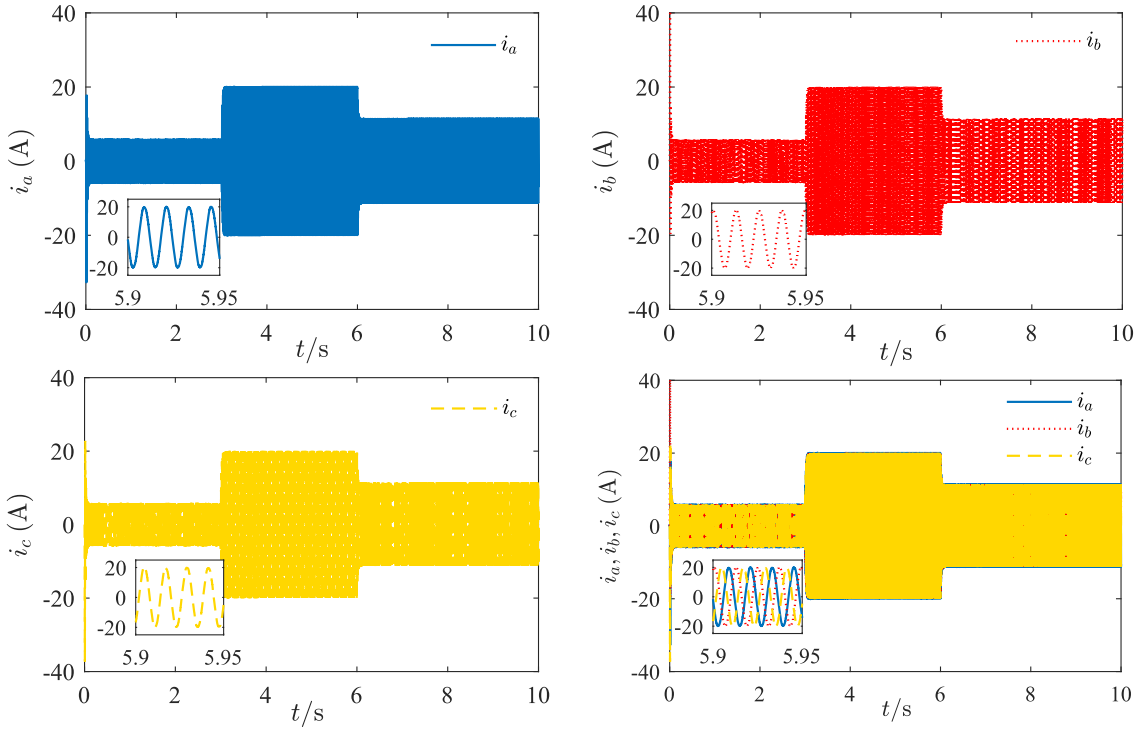

FIGURE 10. Coordination control three - phase current curve.

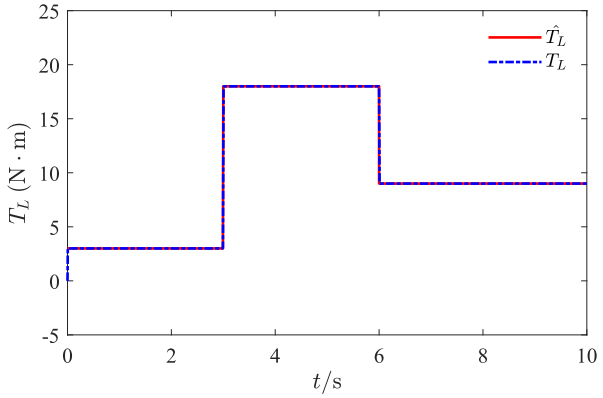

FIGURE 11. Coordination control load torque observation curve.

mode. It can be seen from the zoomed picture that the controller can track the given speed more quickly compared to Fig. 6 and has a smaller output fluctuation compared to Fig. 5. Taking $h = 200$, $k = 2$ in Fig. 8, it can be seen that PMSG under the coordination control can not only quickly track the given desired speed, but also greatly reduce the chattering phenomenon of output. The coordination controller makes full use of the advantages of the two control methods and the control effect is better than that of a single controller, and the output is more stable than that of Fig. 7. Figs. 9-11 show the change curves with respect to time of the torque and three-phase current of PMSG in coordinated control, respectively. The curve of electromagnetic torque has a rapid response and small overshoot, and the torque observer can play a good tracking effect on the uncertain torque parameters. Meanwhile, Figs. 9-11 further verify the effectiveness of the coordination control strategy.

B. SIMULATION OF THE PMSG SYSTEM WITH INPUT SATURATION

The expected speed value of generator is $\omega_r = 29.16$ rad/s when PMSG operates at constant wind speed $v = 18$ m/s. When PMSG is saturated, the anti-saturation auxiliary system starts to take effect. By adjusting the parameters k and h of the coordination function, the coordination controller can quickly eliminate the effect of saturation. The simulation results are shown in Figs. 12-15. In order to reflect the superiority of the coordination control strategy proposed in this paper, we also present the curve of speed trajectory under a single adaptive sliding mode controller in the following simulation.

As can be seen from Fig. 12, when the motor is started, the input current will be too large, resulting in input saturation. The control input of the PMSG system is saturated, the input of i_{qr}^* is limited. The input current does not continue to grow after reaching 4 A, and there is an overshoot phenomenon. After the coordination control, the control input of the system no longer has saturation limit phenomenon, and after saturation compensation, the control input reaches stability at 0.5 s. As can be seen from the Fig. 13 when generator occurs input saturation, under the separate function of the adaptive sliding mode anti-saturation controller, the output of the PMSG system can steadily track the expected speed

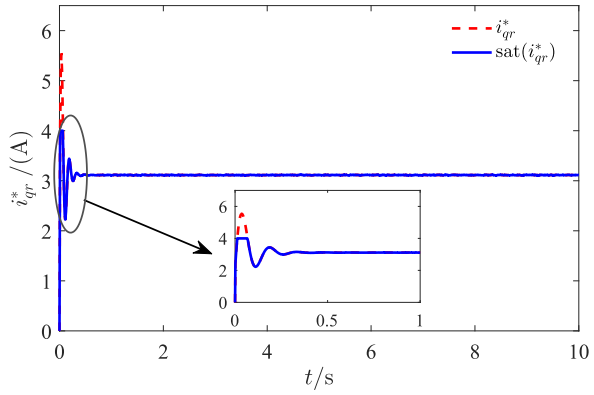

FIGURE 12. Control input curve under saturation constraint.

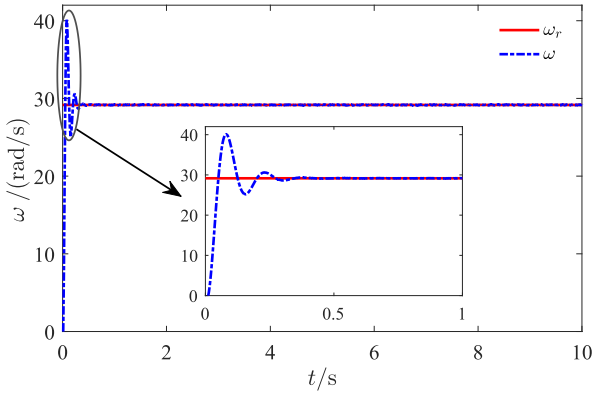

FIGURE 13. Speed curve of adaptive sliding mode anti-saturation control under saturation constraints.

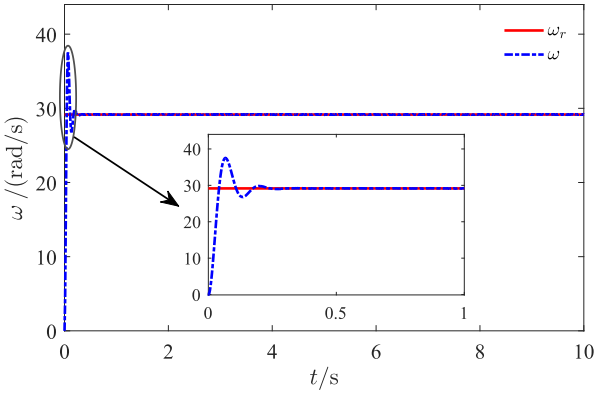

FIGURE 14. Coordination control speed curve under saturation constraints.

value after a brief overshoot fluctuation with satisfactory performance. So the adaptive sliding mode anti-saturation control can quickly compensate for the saturation constraint and realize the speed tracking control. However, the adaptive sliding mode anti-saturation controller is accompanied by large overshoot and poor stability. It can be seen from Fig. 14 that under the coordination control, the speed can quickly track the expected value, and the overshoot phenomenon is weakened compared to Fig. 13. Fig. 15 shows the three-phase

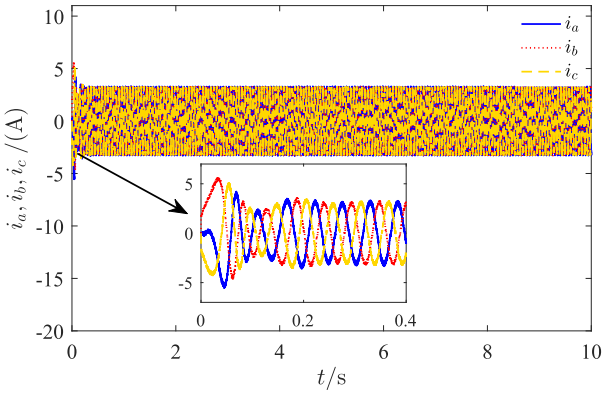

FIGURE 15. Coordination control three-phase current curves under saturation constraints.

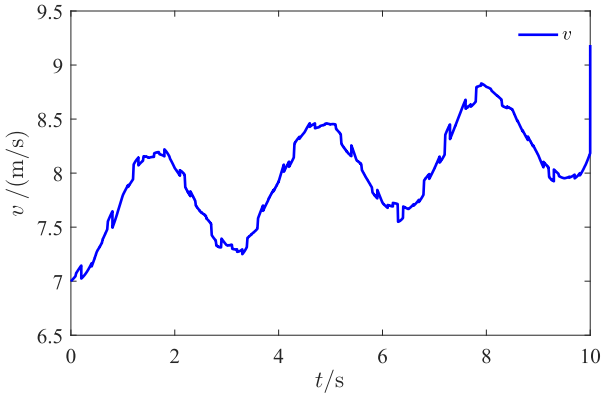

FIGURE 16. Combined wind speed input change curve.

current curve of coordination control under saturation input. It can be seen that in the saturation stage, although the current curve fluctuates, the output can still be stable, which further verifies the effectiveness of the coordination controller.

C. SIMULATION OF THE PMSG SYSTEM UNDER COMBINED WIND SPEED

According to the characteristics of wind speed change, we consider the combined wind speed model [21]. The natural wind divides into basic wind speed components v_b, gust wind speed component v_g, gradual wind speed component v_c and random wind speed component v_n. Therefore, the wind speed v in the wind power plant can be expressed as

$$v = v_b + v_g + v_c + v_n.$$

The change curve of combined wind speed input is given below, and the control effect of coordination control strategy on the PMSG system under combined wind speed is verified.

Fig. 17 is the coordination control speed curve under the combined wind speed input as shown in Fig. 16. It can be seen from the figure that under the influence of the combined wind speed, the output speed of PMSG can still fastly track the given desired speed with small overshoot and output stability. Fig. 18 shows the coordination control speed curve

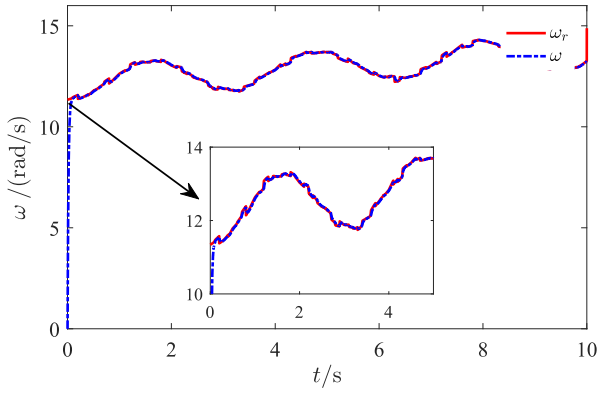

FIGURE 17. Speed curve of coordination control under combined wind speed.

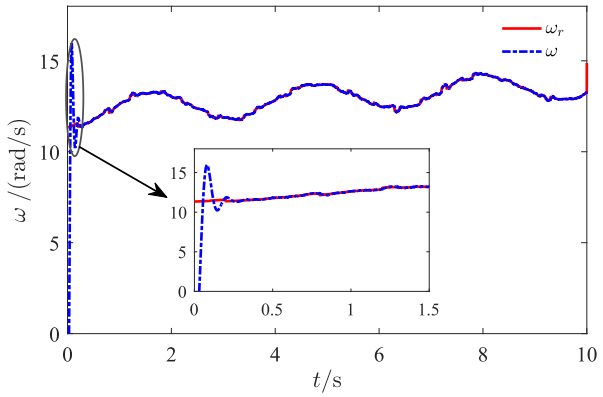

FIGURE 18. Coordination control speed curve under saturation constraints at combined wind speed.

of combined wind speed under saturation constraint. It can be seen from the figure that when the system is saturated, the coordination control strategy under combined wind speed can still make the output of the PMSG system fastly track the given desired speed after a short overshoot and stabilize the output. The fast response performance and anti-saturation ability of the coordination controller are further verified. It can be obtained from the above simulation results, the coordination control strategy adopted in this paper can quickly eliminate the influence of saturation and improve the stability of the system when the input is saturated. It can weaken the overshoot of output to some extent, and the speed tracking control of the PMSG is realized. The proposed control strategy improves the maximum wind energy capture of wind turbine, and further improves the utilization efficiency of wind energy.

Fig. 19 shows the PWM waveform generated by SVPWM control in the simulation. As can be seen from Fig. 19, the switching period of each PWM channel is 1×10^{-4} s, the switching frequency is 10k Hz, and the duty ratio is 0.9.

D. SIMULATION EXPERIMENT

Based on the semi-physical simulation platform, the PMSG system is experimentally studied to verify the rationality

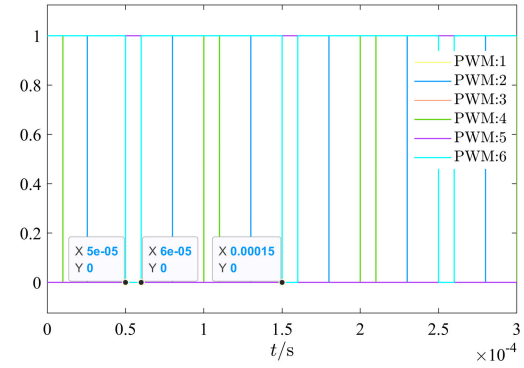

FIGURE 19. PWM waves.

FIGURE 20. Experimental platform of PMSG semi-physical simulation.

TABLE 4. Motor nameplate parameters.

PMSG parameters		
Parameters	**Symbol**	**Value**
Rated power (kW)	P_n	4.5
Rated voltage (V)	U_n	380
Rated current (A)	I_n	12.8
Rated speed (rpm)	R_n	1500
Rated frequency (Hz)	f	50
Rated torque (N · m)	T_n	28.65

and effectiveness of the designed coordination controller. The PMSG semi-physical simulation experiment platform is shown in Fig. 20. The PMSG parameters used in the experiment are shown in Table 4.

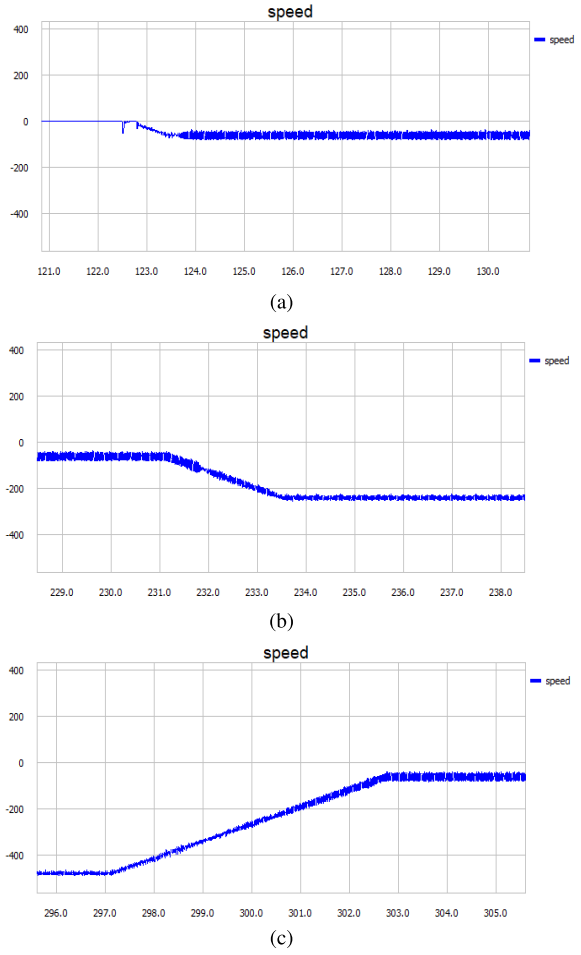

FIGURE 21. Speed output curve of PMSG system.

In the experimental study, the motor speed can be given and changed by setting the frequency of the port corresponding to the frequency converter, and the motor speed is the given input speed. The relation between frequency and motor speed is $n = 60f/p$, where n is the motor speed, f is the generator operating frequency, $p = 5$ is the pole pairs number. Fig. 21(a) shows the output of the generator speed when the frequency of the converter increases from 0Hz to 5Hz, i.e., the speed tracking when the motor starts. Fig. 21(b) shows the output of the generator speed when the frequency of the converter increases from 5Hz to 20Hz, i.e., the speed tracking when the motor accelerates. Fig. 21(c) shows the output of the generator speed when the frequency of the converter decreases from 40Hz to 5Hz, i.e., the speed tracking when the motor decelerates. As can be seen from Fig. 21, the speed of the generator can also track the speed of the motor relatively quickly. However, the generator speed output fluctuates due to friction between the motor and the torque sensor. Fig. 22 shows the output curve of the three-phase current after the generator is connected to the grid. Fig. 22 shows the current waveform has six cycles between 325.4 second and 325.6 second, so the period of each wave is 1/30 s, the angular frequency is 60π rad/s, and the amplitude is 3 A. Therefore,

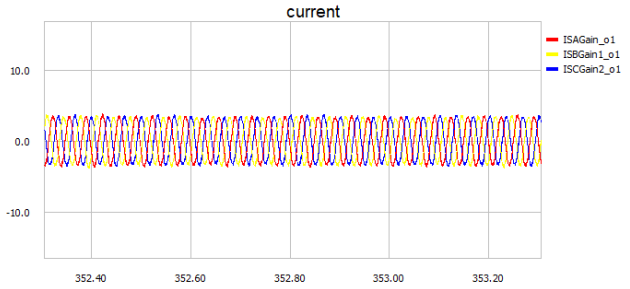

FIGURE 22. Current output curve of PMSG system.

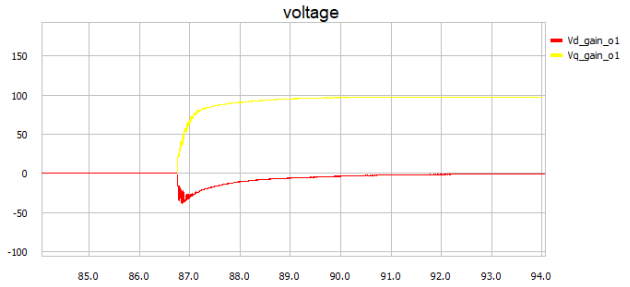

FIGURE 23. Voltage output curve of PMSG system.

the sinusoidal steady-state response of the three-phase current is ISA $= 3\sqrt{2}\cos(60\pi t + \frac{2\pi}{3})$, ISB $= 3\sqrt{2}\cos(60\pi t - \frac{2\pi}{3})$, ISC $= 3\sqrt{2}\cos(60\pi t)$, respectively. Fig. 23 shows the curves of U_d and U_q when the generator is connected to the grid with 0 power. As can be seen from Fig. 23, after the generator is connected to the grid, the q-axis voltage is positive, and the d-axis voltage is maintained near 0, and the voltage output is stable when the generator runs stably. From the above simulation experiment results, it can be seen that the PMSG system can still quickly track the given speed under the controller designed in this paper, which verifies the effectiveness of the controller.

V. CONCLUSION

This paper has proposed a coordination control strategy based on adaptive sliding mode and PCH control methods for the anti-saturation control problem of a permanent magnet synchronous wind power system. In order to solve the problem of saturation and model parameter uncertainty, an adaptive sliding mode controller is designed based on an auxiliary system, and further the PCH controller is designed to reduce output chattering phenomenon caused by sliding mode control. The proposed coordination control strategy makes full use of the advantages of both control methods, which can ensure the system with saturation and model parameter uncertainty has quick dynamic response speed and good steady-state performance so as to optimize the whole control process. The simulation results have illustrated the rationality and effectiveness of the proposed anti-saturation coordination control strategy. One of the next research directions is to find optimal selection range of coordination function to solve the control problem of wind power systems with saturation constraints.

REFERENCES

[1] G. Bandoc, R. Prăvălie, C. Patriche, and M. Degeratu, "Spatial assessment of wind power potential at global scale. A geographical approach," *J. Cleaner Prod.*, vol. 200, pp. 1065–1086, Nov. 2018.

[2] Z. Zheng, Q. Xie, C. Huang, X. Xiao, and C. Li, "Superconducting technology based fault ride through strategy for PMSG-based wind turbine generator: A comprehensive review," *IEEE Trans. Appl. Supercond.*, vol. 31, no. 8, pp. 1–6, Nov. 2021.

[3] W. Sun, Y. Wu, and X. Lv, "Adaptive neural network control for full-state constrained robotic manipulator with actuator saturation and time-varying delays," *IEEE Trans. Neural Netw. Learn. Syst.*, vol. 33, no. 8, pp. 3331–3342, Aug. 2022.

[4] C. Lv, H. Yu, J. Chen, N. Zhao, and J. Chi, "Trajectory tracking control for unmanned surface vessel with input saturation and disturbances via robust state error IDA-PBC approach," *J. Franklin Inst.*, vol. 359, no. 5, pp. 1899–1924, Mar. 2022.

[5] R. Errouissi, A. AI-Durra, and M. Debouza, "A novel design of PI current controller for PMSG-based wind turbine considering transient performance specifications and control saturation," *IEEE Trans. Ind. Electron.*, vol. 65, no. 11, pp. 8624–8634, Nov. 2018.

[6] C. O. Maddela and B. Subudhi, "Robust wide-area TCSC controller for damping enhancement of inter-area oscillations in an interconnected power system with actuator saturation," *Int. J. Electr. Power Energy Syst.*, vol. 105, pp. 478–487, Feb. 2019.

[7] P. Chen, D. Han, and K.-C. Li, "Robust adaptive control of maximum power point tracking for wind power system," *IEEE Access*, vol. 8, pp. 214538–214550, 2020.

[8] J. Wu, J. Zhang, B. Nie, Y. Liu, and X. He, "Adaptive control of PMSM servo system for steering-by-wire system with disturbances observation," *IEEE Trans. Transport. Electrific.*, vol. 8, no. 2, pp. 2015–2028, Jun. 2022.

[9] A. T. Nguyen, M. S. Rafaq, H. H. Choi, and J.-W. Jung, "A model reference adaptive control based speed controller for a surface-mounted permanent magnet synchronous motor drive," *IEEE Trans. Ind. Electron.*, vol. 65, no. 12, pp. 9399–9409, Dec. 2018.

[10] Y. Ren and W. Sun, "Robust adaptive control for robotic systems with input time-varying delay using Hamiltonian method," *IEEE/CAA J. Autom. Sinica*, vol. 5, no. 4, pp. 852–859, Jul. 2018.

[11] L. Pan and C. Shao, "Wind energy conversion systems analysis of PMSG on offshore wind turbine using improved SMC and extended state observer," *Renew. Energy*, vol. 161, pp. 149–161, Dec. 2020.

[12] Y. Wang, Y. Feng, X. Zhang, and J. Liang, "A new reaching law for antidisturbance sliding-mode control of PMSM speed regulation system," *IEEE Trans. Power Electron.*, vol. 35, no. 4, pp. 4117–4126, Apr. 2020.

[13] M. N. Uddin, Z. Zhai, and I. K. Amin, "Port controlled Hamilton with dissipation-based speed control of IPMSM drive," *IEEE Trans. Power Electron.*, vol. 35, no. 2, pp. 1742–1752, Feb. 2020.

[14] G. Wang and W. Sun, "Output tracking of time-delay Hamiltonian descriptor systems under saturation constraints," *J. Franklin Inst.*, vol. 359, no. 7, pp. 2976–2999, May 2022.

[15] J. Chi, H. Yu, and J. Yu, "Hybrid tracking control of 2-DOF SCARA robot via port-controlled Hamiltonian and backstepping," *IEEE Access*, vol. 6, pp. 17354–17360, 2018.

[16] W. Xu, A. K. Junejo, Y. Liu, M. G. Hussien, and J. Zhu, "An efficient antidisturbance sliding-mode speed control method for PMSM drive systems," *IEEE Trans. Power Electron.*, vol. 36, no. 6, pp. 6879–6891, Jun. 2021.

[17] W. Sun, Y. Wu, and L. Wang, "Trajectory tracking of constrained robotic systems via a hybrid control strategy," *Neurocomputing*, vol. 330, pp. 188–195, Feb. 2019.

[18] C. Lv, "A hybrid coordination controller for speed and heading control of underactuated unmanned surface vehicles system," *Ocean Eng.*, vol. 176, pp. 222–230, Mar. 2019.

[19] X. Jiao, Q. Yang, and B. Xu, "Hybrid intelligent feedforward-feedback pitch control for VSWT with predicted wind speed," *IEEE Trans. Energy Convers.*, vol. 36, no. 4, pp. 2770–2781, Dec. 2021.

[20] M. Chen, S. S. Ge, and B. Ren, "Adaptive tracking control of uncertain MIMO nonlinear systems with input constraints," *Automatica*, vol. 47, no. 3, pp. 452–465, Mar. 2011.

[21] S. Li, K. Zhang, J. Li, and C. Liu, "On the rejection of internal and external disturbances in a wind energy conversion system with direct-driven PMSG," *ISA Trans.*, vol. 61, pp. 95–103, Mar. 2016.

DEHAI YU received the B.Eng. degree in electrical engineering and automation from Jining University, Qufu, China, in 2016. He is currently pursuing the M.S. degree in electrical engineering with Qufu Normal University, Qufu. His current research interest includes the control of constrained wind power systems.

WEIWEI SUN received the B.Sc. degree in applied mathematics and the M.Sc. degree in control theory from Qufu Normal University, Qufu, China, in 2002 and 2005, respectively, and the Ph.D. degree in control theory and control engineering from Shandong University, Jinan, China, in 2009. She was a Visiting Scholar with the Department of Electrical and Computer Engineering, University of Virginia, Charlottesville, VA, USA, from 2007 to 2008, and the Department of Computer Science, Brunel University London, Uxbridge, U.K., in 2018. She is currently a Professor with the School of Engineering and the Institute of Automation, Qufu Normal University. She has published over 30 articles in refereed international journals. Her current research interests include nonlinear systems control, constrained system control and its application in wind power systems, and control and application of Hamiltonian systems in network environments.

XIANGYU CHEN received the B.S. degree in applied mathematics from Qufu Normal University, Qufu, China, in 2021, where she is currently pursuing the M.S. degree in control theory. Her current research interests include Hamiltonian systems control and its applications, and adaptive control.

MINGYUAN DU received the B.Eng. degree in electrical engineering from the Shandong University of Science and Technology, China, in 2018. He is currently pursuing the M.S. degree in electrical engineering with Qufu Normal University, Qufu, China. His current research interest includes the control of constrained wind power systems.